Chapter 1 Seasonal Variability of Upwelling near the Southern East China Sea Shelf

1-1 Introduction

The upwelling at the southern East China Sea Shelf has been recognized and studied for years. The upwelling water can be observed as a cold dome at the shelf break northeast of Taiwan (Fan, 1980), drawing much attention because the exchanges between the Kuroshio Water with the East China Sea Shelf Water take place in that region. The upwelling provides a major source of nutrients that support primary production in the East China Sea Shelf (Chen, 1996).

The Kuroshio enters the region along the east coast of Taiwan. After leaving Taiwan, the northward-flowing Kuroshio bifurcates when colliding with the zonal running shelf of the southern East China Sea. The main stream turns east following the topography, while a branch intrudes onto the shelf, bringing the cold and nutrient-rich Kuroshio Subsurface Water to the shelf of the southern East China Sea. The upwelling water contributes a large amount of nutrients to the East China Sea. The contribution is the major source of nutrients to the East China Sea and many times more than the deposits from the Yangtze River (Chen, 1996). Fan (1980) suggested that the cold surface water in this area was originated by the upwelling according to the temperature profiles. The cold water of this upwelling area came from the Kuroshio Subsurface Water that was impeded by the southern East China Sea Shelf (Chern and Wang, 1989).

Although the upwelling phenomenon in the area has been studied for several decades, the temporal variation of upwelling remained discrepant among oceanographers. Based on chemical hydrography, Liu et al. (1992) found that the upwelling in the area occurs year-round, and that it occasionally reaches the sea surface and becomes evident as a cold dome and nutrient-rich surface water. On the other hand, based on a numerical study, Chao (1991) suggested that the path of the Kuroshio shifted with seasonal variation. During the northeast monsoon, the main stream of the Kuroshio was closer to the shelf break while it shifted seaward during the southwest monsoon. The migration of the Kuroshio path will further affect the upwelling; i.e., the upwelling is a seasonal feature. Gong et al. (1997) confirmed that as the Kuroshio path shifted shoreward in winter, the position of the center upwelling also shifted shoreward. Using three shipboard Acoustic Doppler Current Profilers (Sb-ADCP), observations were collected in the different seasons between 1995 and 1997. Tang et al. (2000) further pointed out that an upwelling was always observed during summertime when the Kuroshio moved seaward, but was missing in winter when the Kuroshio moved shoreward.

Recent nutrient data provide a different view about the seasonal variability. Hsu (2005) found that the upwelling intensified during winter and early spring based on high nitrate and phosphate concentration in the euphotic zone. These observational nutrient data are somehow contradictory to the earlier findings. The discrepancy deserves to be further clarified and interpreted. Nevertheless, the seasonal variability cannot be fully resolved from the existing data because of limited spatial and temporal coverage. These phenomena call for renewed modeling efforts with much better resolution. In this study, the seasonal variations of the upwelling as well as their driving mechanisms will be presented and discusses using a fine-grid resolution model with realistic topography and forcing.

1-2 Model description

The Seas Around Taiwan (SAT) model used here is the sigma -coordinate Princeton Ocean Model (POM; Blumberg and Mellor, 1987). The three-dimensional, free surface model solves the primitive equations for momentum, salt, and heat. The SAT model domain extends from 110.5°E to 126°E and from 13.5°N to 28°N. The horizontal grid size is 1/20°, and there are 26 sigma levels in the vertical. At the open boundaries, the SAT model derives its boundary condition from a larger-scale East Asian Marginal Seas (EAMS; Wu and Hsin, 2005) model. The EAMS model has been validated with available observations to date (e.g. Wu and Hsin, 2005; Tseng et al., 2005). Table 1-1 summarizes part of comparisons between model outputs and observations.Wu and Lu (2007) gave a detailed description of the SAT model.

The SAT model was initialized by the temperature and salinity fields of the EAMS model outputs in January 1999, and was thereafter subject to climatological forcing for one year. After the spin-up period, the SAT model was forced with NASA Quick Scatterometer/National Centers for Environmental Prediction (QSCAT/NCEP) wind data sets. Having a temporal resolution of 6 hours and a spatial resolution of 0.5° × 0.5°, the blended QSCAT/NCEP wind stress data set is one of the most up-to-date high-resolution data of ocean surface winds at the present time (Milliff et al., 1999). The SAT model was subject to six-hourly wind stress at the sea surface and the open ocean boundary forcing provided by the EAMS model. The six-hourly NCEP reanalysis V2 sea surface temperature (SST) and monthly sea surface salinity from National Oceanographic Data Center (NODC) were specified at the sea surface of the EAMS model. The simulation period was from 1999 to 2003.

1-3 Result and discussion

Figure 1-1 shows the distribution of the temperatures averaging over a two-month period between April and May in the study area. Figure 1-1a is from the Advanced Very High Resolution Radiometer (AVHRR) SST images in 1999, and Figure 1-1b is the same as Figure 1-1a, but for 2001. A patch of anomalously cold water off northeast Taiwan is found in Figure 1-1a, but not clearly evidenced in Figure 1-1b, indicating that the surface upwelling in the area is an intermittent phenomenon and contains temporal variations. This variation does not have to be a year-to-year variation. Tang et al (2000) pointed out that the upwelling in the region contains several different time scales of temporal variations. Their cruise data showed that the upwelling center might migrate around and with different magnitudes, even in the same season during the different years. The sb-ADCP composite flow pattern also presented a strong intra-seasonal variation in the area.

For comparison and validation, Figure 1-2a shows the averaged temperature at a depth of 20 m between April and May of 1999 from model simulation, while Figure 1-2b is the same as Figure 1-2a, but it is of 2001. The model result shows that a cold dome centered at 25.6°N and 122.1°E is visible off northeast Taiwan in 1999, and its location almost coincides with that shown in the AVHRR SST image (Figure 1-1a). On the other hand, the cold dome is missing in 2001 based on model simulation (Figure 1-2b). This featureless pattern is also consistent with the AVHRR SST image in Figure 1-1b: the upwelling off northeast Taiwan disappears. Furthermore, both the infrared images and model results show that the temperature east of Taiwan is significantly warmer in 2001 than that of 1999. The similarity between satellite and modeled temperatures suggests that the present model is capable of reproducing the temperature patterns in the area.

The time-space structure and relationship between the satellite SST and the modeled temperature are further investigated by the systematic statistical analysis. Figure 1-3 shows correlations between the monthly-mean of satellite SST and the modeled monthly-mean depth-averaged (0~50 m) temperature during the period from 1999 to 2003. The modeled temperature is obviously correlated with the satellite SST with no phase lag. The large correlation coefficients (＞0.9) in the study area demonstrate that the model did capture spatial temperature patterns as well as seasonal upwelling signals similar to observations.

Figure 1-4 shows model-derived flow and temperature patterns at a depth of 20 m on May 1, 1999 when a typical upwelling took place. A cyclonic eddy of about 80 km in diameter is clearly visible off northeast Taiwan. This cyclonic eddy, centered at about 25.35°N and 122.5°E, coincided with the lower temperature area. The temperature near the eddy center was about 3℃ lower than the ambient waters. At about 25°N, the northeastward-flowing Kuroshio with a maximum speed of over 100 cm/s separates away from the continental shelf break. A branch on the inshore side of the Kuroshio intrudes onto the continental shelf. This branch current impeded by the continental margin turns westward and develops as a part of the cyclonic eddy. To calculate the upwelling rate in the area, we have identified an upwelling domain based on a visual inspection of the model-derived flow pattern. The domain, centered near the center of the cyclonic eddy, extends from 122.25°E to 122.75°E in longitude, and from 25.1°N to 25.6°N in latitude (the red box in Figure 1-4). The average upwelling rate over the five-year period is 5.5 m/day in the upper 60 m of the upwelling area. For the upwelling domain of 2800 km^2, the total upwelling transport is about 0.16 Sv (1 Sv=10^6 m^3/s). The values are well in an agreement with the observation-based estimates. Based on chemical hydrography, Liu et al. (1992) presented the first completed descriptions for the upwelling and the estimated rate of 5.4 m/day in the upper 60 m of the upwelling dome based on a box model calculation. Over the upwelling zone with an area of about 2900 km^2, the upwelling volume transport is 0.2 Sv for the calculation (Liu et al., 1992).

The seasonal variability of the upwelling rate is further studied by averaging the vertical velocity from the surface to a depth z. Figure 1-5 shows the monthly averaged vertical velocity in the upper 100 m (solid line), in the top 30 m (dashed line), and in the upper 60 m (open circles). The values of the average vertical velocity in the upwelling area are positive in all months, indicating that the upwelling is a year-round phenomenon which confirms findings by Liu et al (1992). Even though the upwelling occurs year-round, the surface cold dome seems intermittent, due to the fact that the surface signature of the upwelling is occasionally obscured by the Kuroshio water. The values in the upper 60 m have no significant seasonal variation, and range from 6 to 7×10^{-5} m/s (5.2~6.1 m/day). The modeled averaged vertical velocity in March is 5.6 m/day, showing well in an agreement with estimate of Liu et al. (1992) in the same month.

Leaving the layer of the upper 60 m aside, both vertical velocities in the upper 100 m and those in the top 30 m reveal seasonal variability (Figure 1-5). Nevertheless, there is a different seasonal tendency between them. The vertical velocities in summer are stronger than those in winter in the upper 100 m. On the contrary, although averaged over exactly the same domain, the vertical velocities in the top 30 m are stronger in winter than of those in summer. Not only one single mechanism is apparently responsible for this seasonal discrepancy between the upper layer (from the surface to the depth of 100 m) and near-surface layer (up to 30 m). The seasonal tendency in the upper layer resembles that of the previous observations (e.g. Gong et al., 1997; Tang et al., 2000). The present model results confirm that the migration of the Kuroshio has a significant effect on this seasonal variability (Wu and Lu, 2007). In winter, the Kuroshio intrudes onto the shelf of the East China Sea and prevents the formation of the upwelling, and therefore, the vertical velocities in the upper 100 m in the upwelling area are weaker. As the Kuroshio intrusion retreats from the shelf in summer, vertical velocities become stronger.

However, the migration of the Kuroshio fails to explain the seasonal tendency in the top 30 m, where the vertical velocities are stronger in winter and weaker in summer (dashed line in Figure 1-5). The surface layer has heavy interactions with the wind, providing a clue that this different trend in the near-surface layer is due to the seasonal reversal of the monsoonal winds. The winds may affect the sea surface water, causing upwelling and divergence of the surface water. We calculate the upwelling velocity of the Ekman pumping given by

$$w_e = \frac{1}{\rho f}\left(\frac{\partial \tau_y}{\partial x} - \frac{\partial \tau_x}{\partial y}\right) \quad (1)$$

$$\tau = \rho C_D U^2 \quad (2)$$

where w_e is the vertical velocity, ρ = 1.3 kg/m^3 is the density of air, f is the Coriolis parameter, τ is the wind stress, C_D is the drag coefficient, and

U is wind speed at 10m. The value of C_D depends on the prevailing atmospheric conditions. A recently published value for C_D given by Powell et al. (2003) is

$1000C_D = 1.2 \qquad 11m/s \leq U \qquad (3)$

$1000C_D = 0.49 + 0.065U \qquad 11 < U \leq 19m/s \qquad (4)$

The Ekman pumping is then calculated over the summer time and winter time, respectively. The time averaging in summer covers the period from May to July, while winter is from October to December. The Ekman pumping in winter (2.2×10^{-3} m/s) is stronger than that of summer (6.6×10^{-4} m/s), steering a different seasonal tendency in the top 30 m, then making the depth-averaged (0~30 m) vertical velocities in winter stronger than in summer.

Although it is somehow contradictory to the earlier findings, the seasonal variability of this near-surface layer is confirmed by a recent nutrient data set (Hsu, 2005). We have clarified the variation by taking advantage of the new observations in this study. Sequential cruises were conducted over the upwelling region during the period from October, 2003 to November, 2004 (Hsu, 2005). Figure 1-6 shows the nitrate concentration (open circles) together with the modeled vertical velocity (solid squares) in the top 30 m over the upwelling region. The nitrate data adopted here are from Hsu (2005), which are averaged over a two-day period. The averaged data was gathered from several stations within the upwelling region. The modeled vertical velocities are taken with the same dates as the cruises. Similar seasonal tendency has been evidenced in Figure 1-6. The nitrate concentration is generally higher while upwelling is intensified during winter and early spring. The maximum nitrate concentration appears in early April, 2004, coinciding with the maximum vertical velocity taking place. In contrast, summer is usually low in nitrate because of the weakened upwelling.

1-4 Conclusion remarks

This paper presents results from an observation-validated three -dimensional model of the upwelling near the southern East China Sea Shelf. The similarity between the satellite and modeled temperatures suggests that the present model is capable of reproducing the temperature patterns in the area. The values of the average vertical velocity in the upwelling area are positive in all months, indicating that the upwelling is a year-round phenomenon. However, there is a different seasonal tendency between the upper layer (from the surface to the depth of 100 m) and the near-surface layer (up to 30 m). Influenced by the migration of the Kuroshio, the upwelling is stronger in summer than in winter in the upper 100 m. On the other hand, the vertical velocities in the top 30 m are stronger in winter than those of summer, which is attributed to the local wind forcing.

Model provides the upwelling transports in the area which would be beneficial to the oceanographic community for further research. Over the upwelling region with an area of 2800 km^2, the model results show that the average vertical velocity in the top 30 m is 2.8 m/day in summer and 4.2 m/day in winter, while the annual mean is 3.4 m/day. The corresponding upwelling transport is 0.08 Sv in summer, 0.12 Sv in winter, and 0.09 Sv yearly. The average vertical velocity in the upper 100 m is 7.8 m/day in summer, 6.1 m/day in winter, and 6.8 m/day yearly. The upwelling transport in the upper 100 m is 0.21 Sv in summer, 0.17 Sv in winter, and 0.19 Sv yearly.

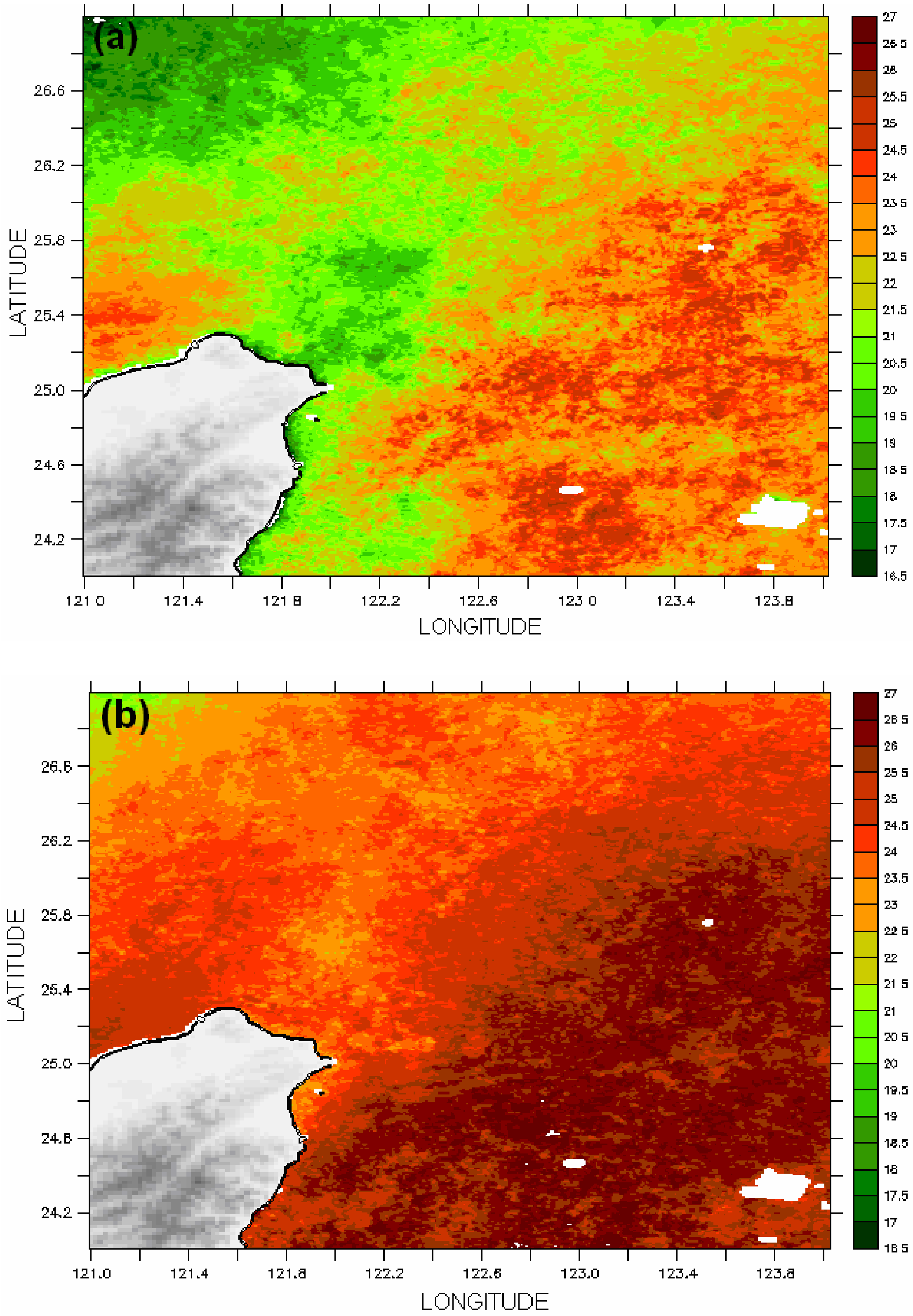

Figure 1-1. Sea surface temperature (SST) averaging between April and May

(a) in 1999, (b) in 2001.

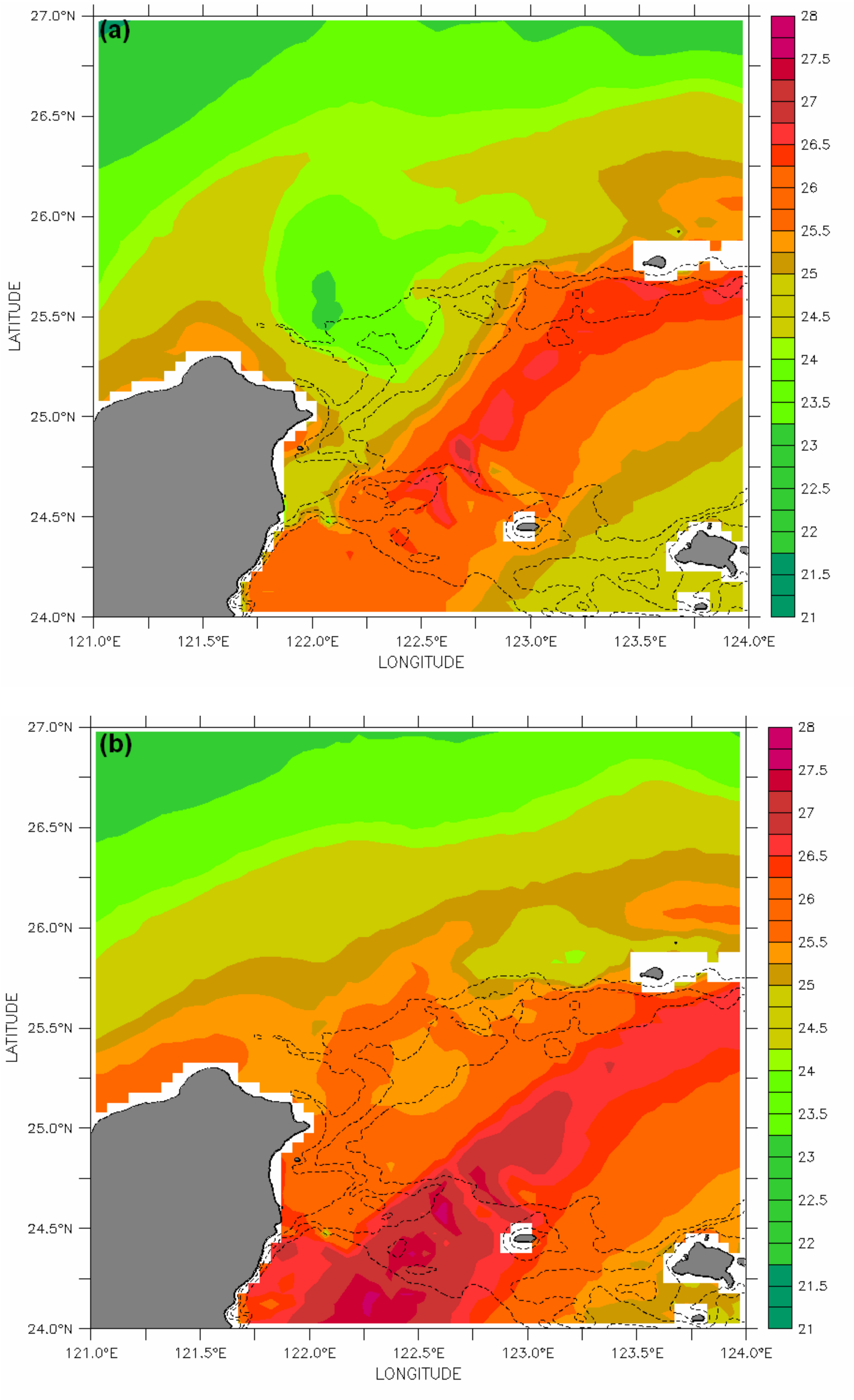

Figure 1-2. Averaged temperature at the depth of 20 m between April and May from the model (a) in 1999, (b) in 2001.

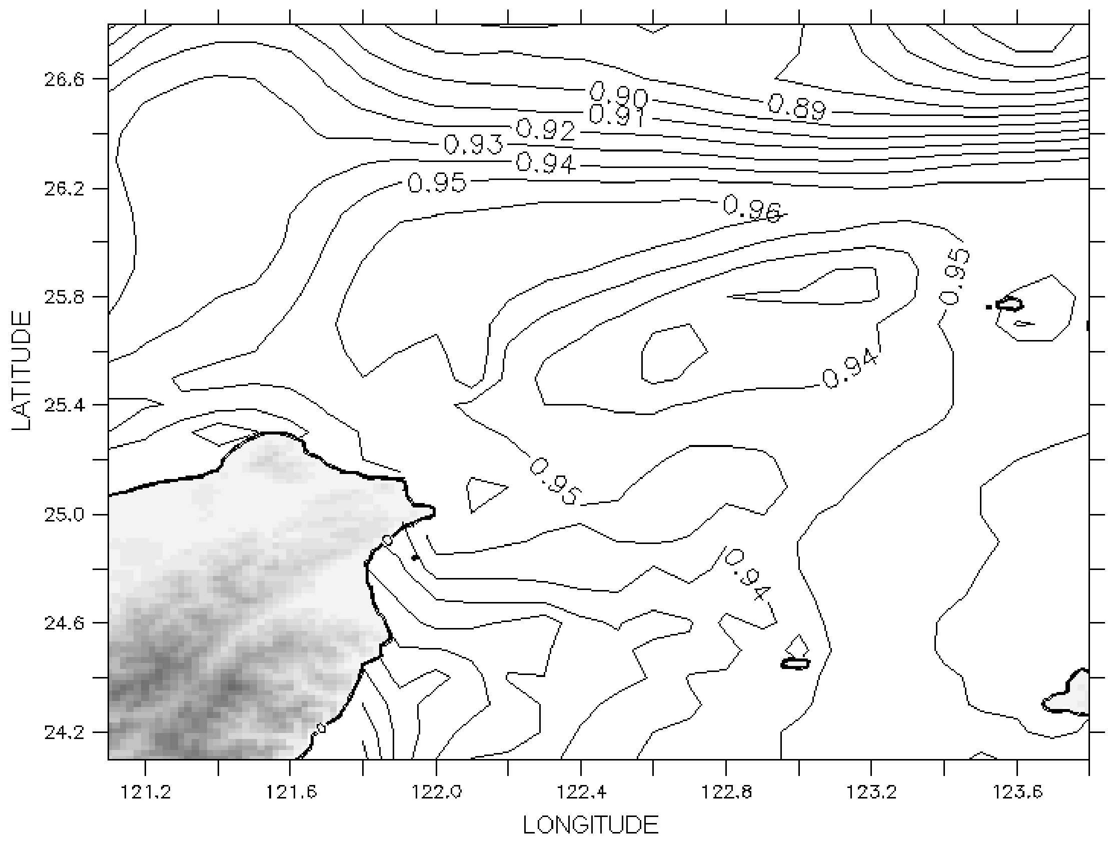

Figure 1-3. Correlations between monthly-mean of satellite SST and the modeled monthly-mean depth-averaged (0~50 m) temperature during the period from 1999 to 2003.

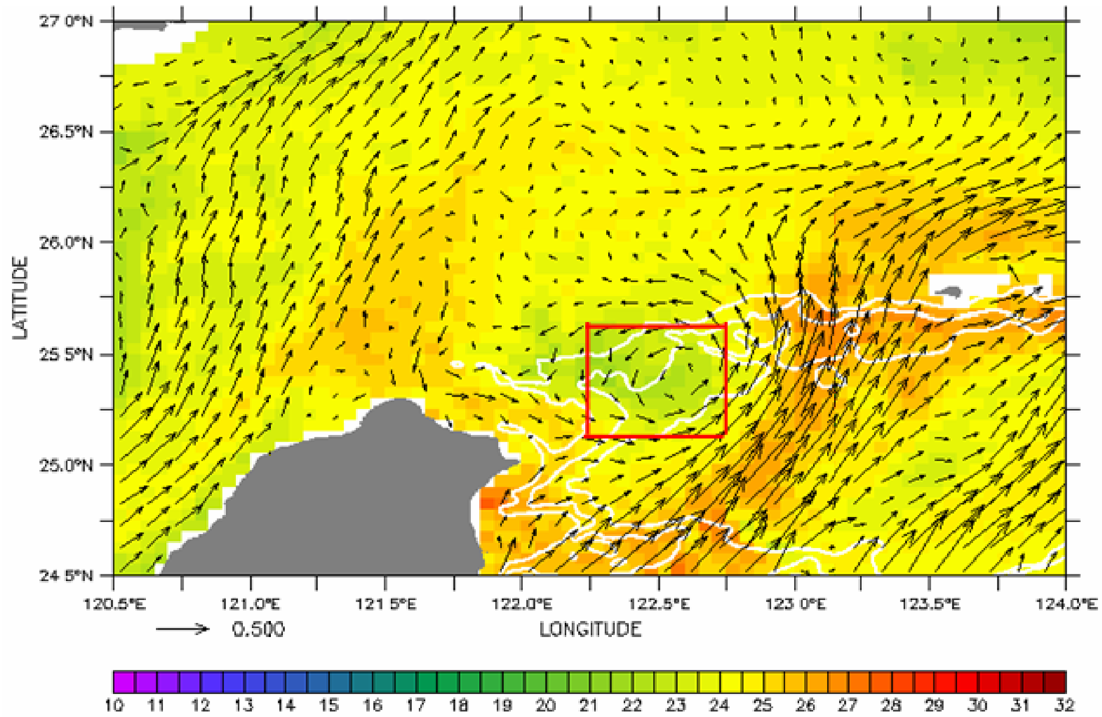

Figure1- 4. Model-derived flow and temperature patterns at depth of 20 m on May 1, 1999. The red box is the upwelling domain which extends from 122.25°E to 122.75°E in longitude, and from 25.1°N to 25.6°N in latitude.

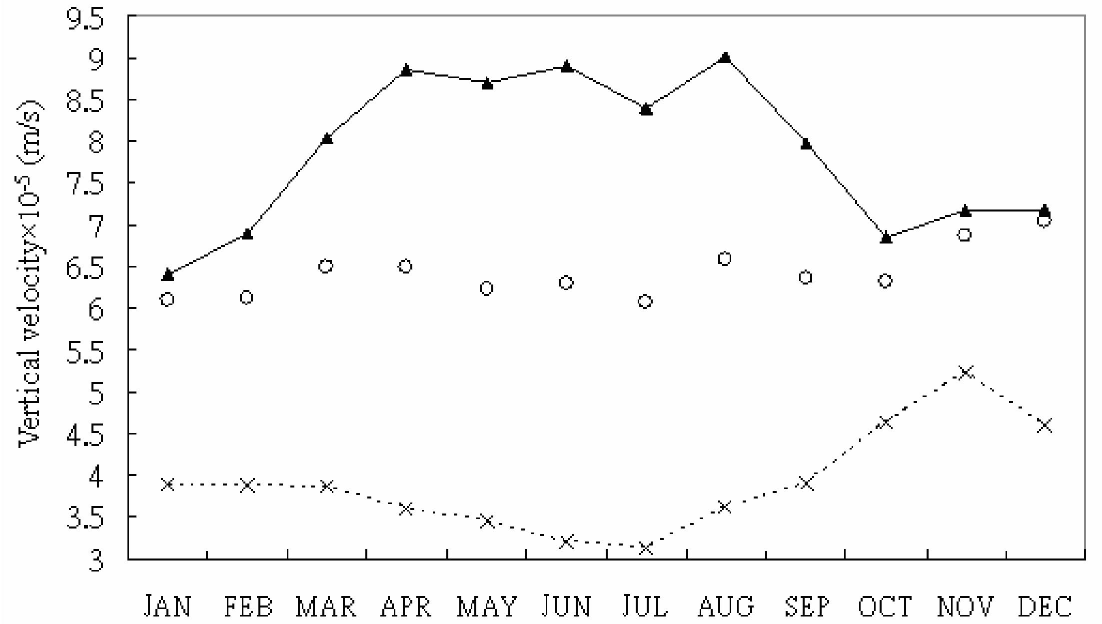

Figure 1-5. Monthly averaged vertical velocity in the upper 100 m (solid line), in the top 30 m (dashed line), and in the upper 60 m (open circles).

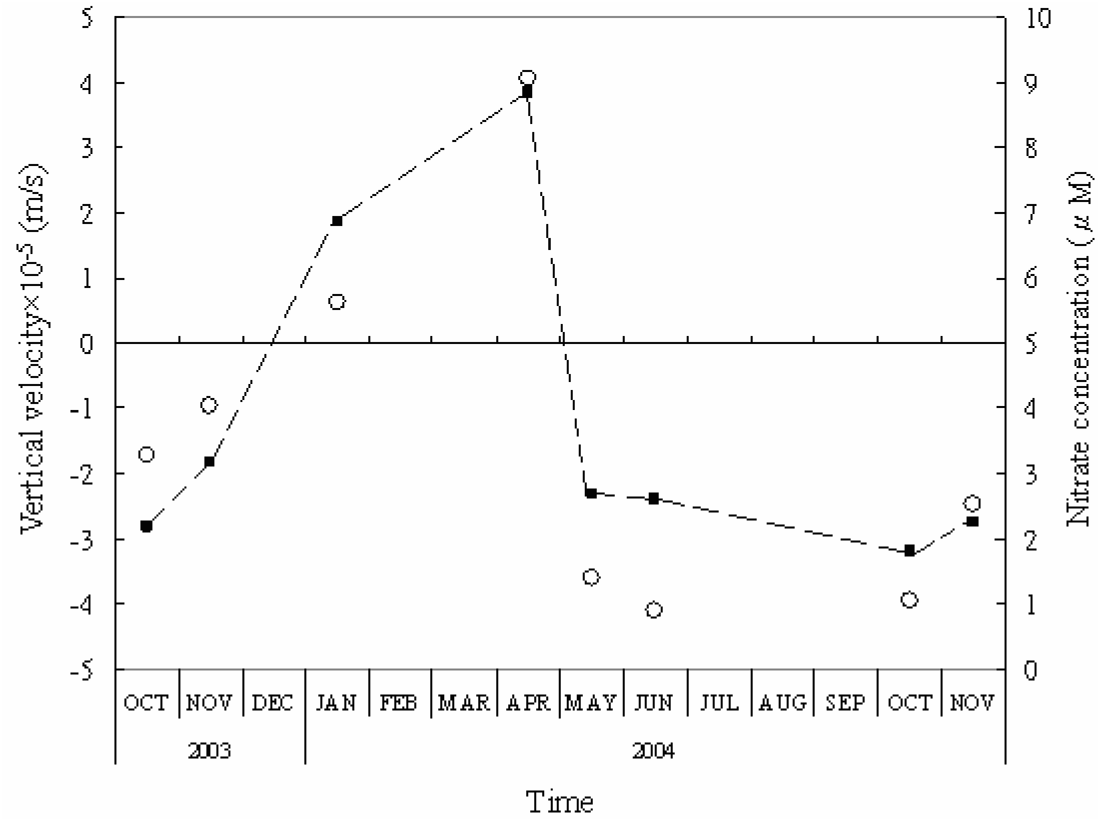

Figure 1-6. The nitrate concentration (open circles; from Hsu, 2005) together with the modeled vertical velocity (solid squares; the same dates as the cruises) in the top 30 m over the upwelling region.

Table 1-1: The quantitative comparison between model outputs and observations

	Location		Model	Observations
Velocity (cm/s)	North Equatorial Current		40	45 (Wyrtki, 1961)
	Southeast of Taiwan		90-100	90 (Gilson and Roemmich, 2002)
	East Taiwan Channel		90-100	100 (Zhang et al., 2001)
	East China Sea		100-110	120 (Yuan et al., 1991)
Transport (Sv)	Kuroshio east of Taiwan		19.7	18.6 (Liang et al., 2003)
	Taiwan Strait	Oct. ~ Nov. 1999	0.11	0.12 (Lin et al., 2005)
		May 1999	1.8	2.0 (Chung et al., 2001)
		Aug. 1999	2.1	2.2 (Chung et al., 2001)
		Aug. 2002	3.0	3.5 (Tseng, 2004)
		Sep. 2003	2.9	3.0 (Tseng, 2004)
	Penghu Channel	Aug. 2002	2.0	2.1 (Tseng, 2004)
		Sep. 2003	1.2	1.2 (Tseng, 2004)
		May 1999	1.5	1.6 (Wang et al., 2004)
		Aug. 1999	1.5	1.58 (Jan and Chao, 2003)
		Oct. 1999	0.75	0.76 (Jan and Chao, 2003)
		Nov. 1999	-0.15	-0.11 (Jan and Chao, 2003)
		Mar. 2000	0.65	0.56 (Jan and Chao, 2003)
		Jun. 2000	1.3	1.26 (Jan and Chao, 2003)
		Aug. 2000	1.7	1.72 (Jan and Chao, 2003)
		Feb. 2001	0	0.02 (Jan and Chao, 2003)
		May 2001	1.2	1.1 (Jan and Chao, 2003)